Polymer Bristles: Adsorption of Low Molecular Weight Poly(oxyethylene)−Poly(oxybutylene) Diblock Copolymers on a Perfluorocarbon Emulsion

Clive Washington*

School of Pharmaceutical Sciences, University of Nottingham, University Park, Nottingham NG7 2RD, U.K.

Stephen M. King

ISIS Facility, Rutherford Appleton Laboratory, Chilton, Didcot, Oxfordshire OX11 0QX, U.K.

David Attwood

School of Pharmacy, University of Manchester, Oxford Road, Manchester M13 9PL, U.K.

Colin Booth, Shao-Min Mai, and Yung-Wei Yang

Department of Chemistry, University of Manchester, Oxford Road, Manchester M13 9PL, U.K.

Terence Cosgrove

School of Chemistry, University of Bristol, Cantock's Close, Bristol BS8 1TS, U.K.

Received May 11, 1999; Revised Manuscript Received December 16, 1999

ABSTRACT: We report the results of a small-angle neutron scattering study into the structure of the adsorbed layers formed at the interface in a dilute perfluorodecalin-in-water emulsion by five short chain diblock copolymers of oxyethylene (OE) and oxybutylene (OB) ($OE_{26}OB_{13}$, $OE_{29}OB_{11}$, $OE_{30}OB_{7}$, $OE_{27}OB_{6}$, and $OE_{58}OB_{13}$). The results are discussed in the context of the Marques−Joanny−Leibler scaling description of block copolymer adsorption from selective solvents and provide an insight into the validity of the theory in the unusual limit of short chain lengths and small anchor blocks, close to the boundary between the buoy-dominated and the van der Waals−buoy regimes. The volume fraction profiles are best described by parabolic and, to a lesser extent, Gaussian functional forms. When the temperature was increased, the buoy blocks were found to contract toward the surface, giving rise to profiles that were more blocklike, in accordance with theoretical predictions by Wijmans and Zhulina (*Macromolecules* **1993**, *26*, 7214).

Introduction

Improving our understanding of how surfactant and copolymer molecules arrange themselves at interfaces, particularly in colloidal systems, both is of fundamental interest and is important in a wide range of technological processes and biomedical applications.[1−3] Block copolymers have been particularly widely studied in this regard because they provide a means of achieving two mutually exclusive requirements; the need for a strongly adsorbed *anchor* (A) block and a well-solvated *buoy* (B) block. At an impenetrable interface, AB-type *diblock* copolymers tend to be more effective in this role than ABA-type *triblock* copolymers of the same overall length, or the same buoy block length, since the nonadsorbing segments in the latter are predominantly in the form of loops. These loops possess less configurational entropy than the tails present in an adsorbed layer formed by diblock or BAB-type (effectively "double-diblock") copolymers. However, if the solvent is selectively poor for one block, copolymer micelles or micellar networks may form. Adsorption from selective solvents can therefore lead to competition for material between the processes of adsorption and micellization provided that the latter is not irreversible.

For aqueous systems arguably the most widely studied buoy block is poly(oxyethylene) (POE).[4−7] Copolymers of POE with alkyl chains (C_iOE_m or Brij) or poly(oxypropylene) (Pluronic, Synperonic, or Poloxamer for BAB materials and Pluronic-R for ABA materials) are available commercially. A particular problem with the POE/POP copolymers is that the acidity of the tertiary proton in propylene oxide gives rise to a transfer reaction during polymerization.[8] This leads to a range of polymeric impurities[9] which can only be completely removed under carefully controlled laboratory conditions.[10] Consequently published work on these materials is based on samples of rather variable purity. This can be overcome by using poly(oxybutylene) (POB) in place of POP. A range of high-purity POE/POB block copolymers have been synthesized and characterized by Booth and co-workers in recent years,[11−13] and these materials have also started to appear commercially (Dow B−Series Polyglycols). An added benefit is that POB is at least four to six times more hydrophobic than POP, giving rise to much better delineated solution phase behavior, though micellization should still be completely reversible under normal experimental conditions since the glass transition temperatures of the constituents are below 210 K.

In this work we have used small-angle neutron scattering (SANS) to examine the structure of the adsorbed layers formed by a number of POE−POB diblock copolymers at the perfluorocarbon−water interface in a submicron emulsion, a model colloidal

10.1021/ma990730v CCC: $19.00
Published on Web 01/31/2000

system we have used previously.[14,15] Compared to polymer latices or the inorganic oxide sols more traditionally associated with adsorption studies, a perfluorocarbon emulsion has some particularly useful features: (i) the neutron scattering length density of the perfluorocarbon can still be contrast-matched to a D_2O-rich medium, (ii) the emulsion droplet offers a homogeneous, molecularly smooth, spherical surface which, because the hydrogenous copolymers are not soluble in the perfluorocarbon, may be regarded as impenetrable (i.e., solid), and perhaps most importantly, (iii) because of the high density of the perfluorocarbon (1.94 g cm^{-3}) the emulsion droplets are easily sedimented by centrifugation, allowing unadsorbed copolymer to be removed by washing and the droplets resuspended in water without excessive coalescence. As a result, it is possible to gather high-quality scattering data from just the adsorbed copolymer layers with a negligible contribution from free or micellar copolymer in the bulk phase, or from the dispersed phase itself.

Experimental Section

Materials. Perfluorodecalin and perfluoroperhydrophenanthrene were kindly provided by Rhone-Poulenc ISC Division (now BNFL Fluorochemicals), Bristol, U.K., and were used as received. Both materials were at least 99.5 at. % F and had isomeric purities greater than 95%. Deuterium oxide, 99.9 at. % D, was purchased from CDN Isotopes, Canada. Ethylene oxide and 1,2-butylene oxide were obtained from Fluka Ltd and were dried and distilled immediately before use.

Preparation and Characterization of Copolymers. The general methods of polymerization and characterization of POE/POB copolymers have been described previously.[11,16] Briefly, the copolymers were prepared by sequential polymerization of ethylene oxide (EO) followed by 1,2-butylene oxide (BO) as follows. To form the initiator, 2-(2-methoxyethoxy)ethanol ($CH_3OCH_2CH_2OCH_2CH_2OH$) was reacted with freshly cut potassium metal to form a solution of its salt ($OH/K^+ = 15$). A portion of this initiator solution was injected by syringe under dry nitrogen flow into a previously flamed ampule fitted with a Teflon tap, and the required amount of EO transferred in via a vacuum line. The ampule was immersed in a water bath successively at 45 and 65 °C until all the EO was polymerized (ca. 2 weeks). After removal of a small sample for analysis, the required amount of BO was then transferred into the ampule, which was left in the water bath at 65−80 °C for a further 2 weeks. Total consumption of monomer in a given stage was verified by cooling the upper part of the ampule with a pellet of solid CO_2 and checking for condensation. Gel permeation chromatography (GPC), calibrated with poly(oxyethylene) standards, gave the polydispersity, expressed as the ratio of mass-average to number-average molar mass (M_w/M_n). The measured polydispersities correspond to a standard deviation in the quoted *combined* block lengths of up to nine monomer units. ^{13}C NMR spectroscopy gave the overall composition and true values of M_n and hence molecular formulas for the copolymers. Comparison of the integrals of resonances from end group and OE/OB-junction carbons verified the diblock structure.

The molecular characteristics of the copolymers are summarized in Table 1. Estimates for the radii of gyration, R_g, of the OE blocks have been derived by extrapolation from published data.[17] The critical micelle concentrations (cmcs) of the copolymers, which are relatively insensitive to OE block length, have been estimated using a recent correlation with the OB block length,[18] and range from 2 to 0.003 mmol dm^{-3} at 30 °C (approximately corresponding to cmcs of 0.3% w/v for $OE_{27}OB_6$ and 0.001% w/v for $OE_{58}OB_{13}$).

Preparation of Emulsion. The emulsion was prepared by homogenizing 10% v/v perfluorodecalin and 2% v/v perfluoroperhydrophenanthrene in the appropriate copolymer solution at 4% w/v (i.e., above the cmc) using an ultrasonic probe (Dawe Soniprobe) at a power of approximately 25 W. Perfluoroperhydrophenanthrene is a fluorocarbon oil which is completely miscible with perfluorodecalin and which reduces the rate of Ostwald ripening of the droplets.[19] The emulsions were then transferred to a dispersion medium of the appropriate scattering length density by gentle centrifugation (1000*g* for 20 min) followed by redispersal in a mixture of 28% w/w H_2O/72% w/w D_2O (the exact point of contrast match was optimized in situ on the neutron beamline). This procedure was repeated three times to ensure that the disperse phase H:D composition was not only correct but also, as far as practicable, free of unadsorbed and micellar copolymer. The final phase volume of the emulsions was in the range 4−5% v/v and was determined from the density of the emulsion as described previously.[14]

Table 1. Molecular Characteristics of Copolymers[a]

	M_n (g mol^{-1})	M_w/M_n	ω_{OE}	ν_B	$R_{g,OE}$ (nm)	β_{sel}
$OE_{26}OB_{13}$ $N_B = 26$, $N_A = 25$	2080	1.05	0.550	0.510	1.25	1.14
$OE_{29}OB_{11}$ $N_B = 29$, $N_A = 21$	2070	1.05	0.620	0.580	1.3	1.33
$OE_{30}OB_7$ $N_B = 30$, $N_A = 13$	1830	1.05	0.720	0.698	1.35	1.73
$OE_{27}OB_6$ $N_B = 27$, $N_A = 11$	1620	1.05	0.730	0.710	1.3	1.76
$OE_{58}OB_{13}$ $N_B = 58$, $N_A = 25$	3490	1.04	0.730	0.699	2.0	1.85

[a] M_n is the number-average molar mass, ω_{OE} is the weight-fraction of OE blocks as determined by NMR and given by $M_{OE}/(M_{OE} + M_{OB})$, ν_B is the number fraction of buoy segments given by $N_B/(N_A + N_B)$ (see the Appendix), and R_g is the estimated radius-of-gyration of the OE blocks (see Experimental Section). β_{sel} Is the block asymmetry parameter (see eq 4 in the main text).

The size distributions of the emulsion droplets were measured by dynamic light scattering (Malvern 4700 PCS using the cumulants method and CONTIN for the distribution analysis). The characteristics of the emulsions formed with each copolymer are given in Table 2.

Small-Angle Neutron Scattering. SANS data were obtained on the LOQ small-angle diffractometer at the ISIS Spallation Neutron Source (Rutherford Appleton Laboratory, Didcot, U.K.).[20,21] This is a fixed-geometry "white beam" time-of-flight instrument which utilizes neutrons with wavelengths, λ, between 0.2 and 1 nm to provide a simultaneous Q range of 0.08−16 nm^{-1}. The scattering vector, Q, which is the independent variable in the measurements is defined as

$$Q = \frac{4\pi}{\lambda}\sin\left(\frac{\theta}{2}\right)$$

where θ is the scattering angle.

Method. To reduce multiple scattering effects, each emulsion sample was diluted to a disperse phase fraction of 4−5% v/v. A portion of a diluted sample was centrifuged for 15 min at 13000*g* to sediment the dispersed phase in order that the supernatant could be used as a background. Each sample and background was placed in 2 mm path length quartz cuvettes and was measured for a total of 4 h but in 1 h runs in order to gather data of high statistical precision. Visual examination of the samples, and examination of the initial and final scattering curves, showed no evidence of sample degradation, coalescence, or sedimentation during this period, so the 1 h data sets were combined prior to analysis. Measurements were performed at 25, 44, and 62 °C.

Each raw scattering data set was corrected for the sample transmission and background scattering and converted to scattering cross-section data ($\partial\Sigma/\partial\Omega$ vs Q) using the instrument-specific software.[22] These data were placed on an absolute scale (cm^{-1}) using the scattering from a standard sample (a solid blend of hydrogenous and perdeuterated polystyrene) in accordance with established procedures.[23]

Table 2. Physical Characteristics of the Fluorocarbon Emulsions

	$OE_{26}OB_{13}$	$OE_{29}OB_{11}$	$OE_{30}OB_7$	$OE_{27}OB_6$	$OE_{58}OB_{13}$
emulsion phase fraction, ϕ	0.051	0.045	0.050	0.044	0.045
volume mean diameter (nm)[a]	361	294	368	224	208
surface mean diameter (nm)[a]	342	272	340	202	200
polydispersity[b]	0.15	0.05	0.15	0.11	0.12

[a] The volume and surface mean diameters were computed from the (measured) intensity-weighted diameters by the instrument software. [b] The polydispersity of a particulate system is defined as the relative standard deviation of the log-normal distribution using cumulants analysis.

Data Analysis. Under the conditions that the perfluorocarbon oil phase and dispersion medium are at contrast match, ignoring any contribution from fluctuations in the average layer structure, the scattering from the copolymer layer can be described by a surface-Guinier type function which has the form[24,25]

$$(\partial\Sigma/\partial\Omega)(Q)\ (\mathrm{cm}^{-1}) = [(6 \times 10^{-22})\pi(\rho_p - \rho_s)^2\phi(Rd^2)^{-1}](\Gamma/Q)^2 \exp(-Q^2\sigma^2) + \text{background} \quad (1)$$

where ρ_p is the scattering length density of the copolymer (in cm^{-2}) and ρ_s is the scattering length density of the (matched) droplet cores and dispersion medium, ϕ is the volume fraction of droplets, R is the mean radii of the droplets (in Å), and d is the bulk density (of the copolymer in this instance; in $\mathrm{g\ cm}^{-3}$). The leading term between square brackets is thus a constant for a given emulsion. The remaining quantities are as follows: Γ, the mass of copolymer adsorbed per unit area or "adsorbed amount" (in $\mathrm{mg\ m}^{-2}$) and σ, the distance of the center-of-mass of the adsorbed copolymer layer from the interface or "second moment" (in Å). Equation 1 is valid when $Q\sigma < 1$.

Estimates for Γ and σ were found by nonlinear least-squares fitting of the scattering data in the region $0.08 < Q\ (\mathrm{nm}^{-1}) < 0.8$. With the exception of the Q-independent background, all other parameters were constrained to their experimental values. Our previous paper[14] discusses the errors inherent in the estimation of these parameters, which are on the order of 5%. Values for the scattering length densities of the copolymers and the dispersion medium at 25 °C were obtained from appropriate weighted sums of the values for POE ($+0.637 \times 10^{10}\ \mathrm{cm}^{-2}$ for $d = 1.127\ \mathrm{g\ cm}^{-3}$) and POB ($+0.195 \times 10^{10}\ \mathrm{cm}^{-2}$ for $d = 0.975\ \mathrm{g\ cm}^{-3}$) and for H_2O ($-0.559 \times 10^{10}\ \mathrm{cm}^{-2}$ for $d = 0.997\ \mathrm{g\ cm}^{-3}$) and D_2O ($+6.355 \times 10^{10}\ \mathrm{cm}^{-2}$ for $d = 1.105\ \mathrm{g\ cm}^{-3}$), respectively. The scattering length density of perfluorodecalin is $+4.183 \times 10^{10}\ \mathrm{cm}^{-2}$ ($d = 1.940\ \mathrm{g\ cm}^{-3}$).

Two approaches have been used to obtain the copolymer volume fraction profiles, $\Phi(z)$, that describe the average distribution of segments in the interfacial region.[26] The first was the Hilbert transformation method of Crowley,[27] a procedure which we have used previously with POE−POP−POE copolymers[14,15] and which yields a *model-independent* profile consistent with the data. However, on this occasion, we were unhappy with the degree of statistical noise on the profiles obtained by this route. We are unsure of the reason for this, but as will become apparent, the profile types and molecular weights are rather different in the two cases and so it may simply be a sensitivity problem. For this reason we have also used an indirect model-fitting procedure developed by Cosgrove.[28] In this approach a parametrized mathematical form for the volume fraction profile is back-transformed into scattering data which is then compared to the experimental scattering data. Iteration of the parameters then obtains the profile *of the chosen mathematical form* that best describes the data. It must be stressed here that although modern theoretical descriptions of copolymer adsorption can be used to guide the selection of profiles, the only reliable methodology is to test several individual functional forms for $\Phi(z)$ on each experimental data set.

Given a volume fraction profile, it is then possible to derive several estimates of the thickness of the adsorbed layer and also the fraction of bound copolymer segments by integrating the area between the surface and $z = 1.3$ nm.[29] This outer limit corresponds to the extent of one lattice layer in a Scheutjens−Fleer self-consistent field model of polymethylene adsorption;[30,31] i.e., it is assumed that polymethylene is a reasonable representation of poly(oxyethylene).

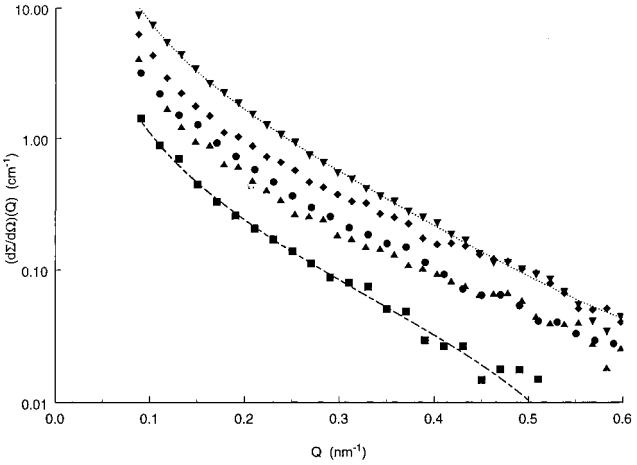

Figure 1. SANS data from the adsorbed copolymers at 25 °C: (●) $OE_{26}OB_{13}$; (▲) $OE_{29}OB_{11}$; (■) $OE_{30}OB_7$; (◆) $OE_{27}OB_6$; (▼) $OE_{58}OB_{13}$. Also shown are a fit of eq 1 to the $OE_{30}OB_7$ data (− −) and the scattering data representing the best-fit parabolic volume fraction profile for the $OE_{58}OB_{13}$ data (· · ·).

Results

Figure 1 shows the scattering data from the adsorbed copolymers in the Q regime of interest. These data were obtained at 25 °C. At low-Q the data decay as approximately Q^{-2}, the expected behavior for scattering from a thin spherical shell. Above $Q > 0.4\ \mathrm{nm}^{-1}$ the signal approaches background levels. Copolymers $OE_{29}OB_{11}$, $OE_{27}OB_6$, and $OE_{58}OB_{13}$ were also studied at 44 and 62 °C, but these data are rather similar to those shown in the figure and so have been omitted for clarity. An example of a surface-Guinier fit of eq 1 to the data for $OE_{30}OB_7$ is shown, however, and is representative of these fits in general. The results of the surface-Guinier analysis are given in Table 3. This table also shows the surface density, θ, of adsorbed chains derived from the adsorbed amount according to

$$\theta\ (\mathrm{nm}^{-2}) = 6.022 \times 10^{23} \times 10^{-21} \times \Gamma\ (\mathrm{mg\ m}^{-2})/M_n\ (\mathrm{g\ mol}^{-1}) \quad (2)$$

and the corresponding interchain separation, D, assuming homogeneous coverage. Since the average size of a polymer molecule in solution is approximately twice its radius of gyration, it follows that adsorbed chains will begin to interact laterally with one another when $R_g \geq D$. Thus, the smaller the ratio D/R_g, the more steric perturbation neighboring chains will exert on one another.

Four different types of volume fraction profile have been tested against each data set; a parabolic profile of

Table 3. Results of the Surface Guinier Analysis of the Scattering Data (eq 1)[a]

	T (°C)	Γ_{SANS} (mg m^{-2})	θ_{SANS} (nm^{-2})	D (nm)	$D/R_{g,OE}$	σ_{SANS} (nm)
$OE_{26}OB_{13}$	25	2.17 ± 0.03	0.63	1.3	1.02	2.15 ± 0.05
$OE_{29}OB_{11}$	25	1.79 ± 0.03	0.52	1.4	1.05	1.54 ± 0.09
	44	1.83 ± 0.02	0.53	1.4	1.03	1.56 ± 0.06
	62	1.66 ± 0.05	0.48	1.5	1.09	1.65 ± 0.14
$OE_{30}OB_{7}$	25	1.37 ± 0.03	0.45	1.5	1.10	1.68 ± 0.10
$OE_{27}OB_{6}$	25	2.20 ± 0.02	0.82	1.1	0.87	1.46 ± 0.06
	44	2.24 ± 0.02	0.83	1.1	0.86	1.40 ± 0.04
	62	2.24 ± 0.02	0.83	1.1	0.86	1.10 ± 0.07
$OE_{58}OB_{13}$	25	2.93 ± 0.02	0.51	1.4	0.72	2.36 ± 0.02
	44	2.90 ± 0.02	0.50	1.4	0.72	2.11 ± 0.03
	62	2.93 ± 0.03	0.51	1.4	0.72	2.02 ± 0.05

[a] Γ_{SANS} is the measured adsorbed amount, θ_{SANS} and D are the surface density and the distance between adsorbed chains, respectively, derived from Γ_{SANS}, and σ_{SANS} is the measured second moment of the adsorbed layer.

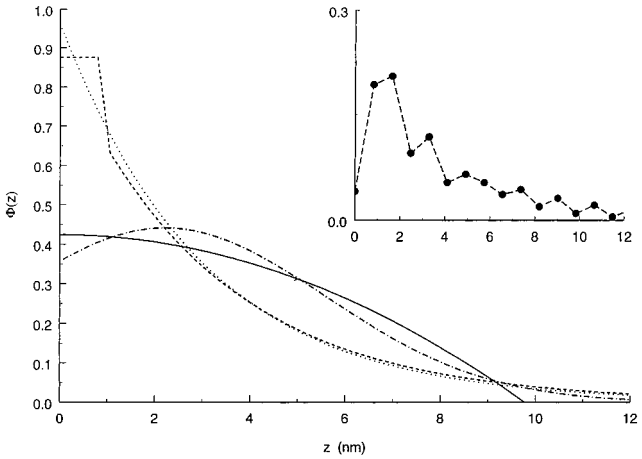

Figure 2. Volume fraction profiles tested against the 25 °C $OE_{58}OB_{13}$ data. The parabolic profile (continuous line) describes the data best. For comparison the inset shows the model-independent profile derived by direct inversion of the scattering data.

the form $\Phi(z) = U - Vz^2$ (where U and V are scalars), a Gaussian, an exponential, and a combination of a rectangular block 1 nm wide followed by an exponential. A justification for these selections is given in the discussion below, but examples for $OE_{58}OB_{13}$ at 25 °C are depicted in Figure 2. For comparison this also shows the corresponding profile derived by direct inversion of the scattering data. The physical parameters describing these various profiles, obtained from the model-fitting procedure, are given in Tables 4−7 . In these, δ_{rms} is the rms thickness of the layer, related to σ through

$$\sigma = \delta_{rms} - \frac{\int \Phi(z)\, z\, dz}{\int \Phi(z)\, dz} \qquad (3)$$

δ_h is the maximum extent, or span, of the layer (essentially the hydrodynamic thickness), and $\langle p \rangle$ is the bound fraction. The magnitude of the statistical χ parameter is also shown. We wish to emphasize that the values of Γ and σ shown in Tables 4−7 were obtained by iteration; they were not constrained at the values obtained from the surface-Guinier analysis *with which they should be directly compared*.

Discussion

Adsorbed Amount and Layer Thickness. A careful examination of the data in Table 3 reveals no correlations in the data between θ (or Γ) and the composition of the copolymers or the overall molecular weight. There is some evidence that σ increases with increasing molecular weight, but curiously, it does not scale with the length of the POE buoy block alone. What all this would appear to suggest is some rather complex interfacial behavior which we will examine shortly within the framework of the scaling description for block copolymer adsorption from *selective* solvents as proposed by Marques, Joanny, and Leibler (hereafter MJL).[32]

There is very little published literature concerning the *adsorption* of diblock POE−POB copolymers. Schillen et al. have studied $OE_{41}OB_8$ adsorbing on hydrophobic silica,[33] and Griffiths et al. have studied $OE_{100}OB_{15}$ and $OE_{200}OB_{15}$ adsorbing on polystyrene latex.[34] These all had pseudo-plateau adsorbances in the region 1.4 to 1.8 mg m^{-2} which are of a similar magnitude to the data we report in Table 3; though in our previous work with

Table 4. Parameters Derived from Model-Fitting Volume Fraction Profiles to the Scattering Data: Parabolic-Type Profiles[a]

	T (°C)	χ^2	Γ (mg m^{-2})	σ (nm)	δ_{rms} (nm)	δ_h (nm)	$\langle p \rangle$
$OE_{26}OB_{13}$	25	0.63	2.17	1.87	3.40	7.48	0.21
$OE_{29}OB_{11}$	25	0.41	1.86	1.87	3.41	7.50	0.21
	44	0.43	1.84	1.46	2.66	5.86	0.27
	62	0.49	1.66	1.28	2.33	5.18	0.30
$OE_{30}OB_{7}$	25	0.33	1.39	1.87	3.40	7.48	0.21
$OE_{27}OB_{6}$	25	0.47	2.20	1.35	2.46	5.45	0.28
	44	0.42	2.27	1.67	3.03	6.67	0.24
	62	0.26	2.24	1.08	1.97	4.37	0.35
$OE_{58}OB_{13}$	25	0.50	2.98	2.39	4.36	9.48	0.18
	44	0.58	2.94	2.15	3.91	8.60	0.19
	62	0.42	2.96	2.05	3.73	8.21	0.19

[a] Γ is the adsorbed amount, σ is the second moment of the volume fraction profile, δ_{rms} is the rms extent of the profile, δ_h is the span of the profile (approximately equivalent to the hydrodynamic thickness), and $\langle p \rangle$ is the fraction of copolymer segments lying within 1.3 nm of the interface.

Table 5. Parameters Derived from Model-Fitting Volume Fraction Profiles to the Scattering Data: Gaussian-Type Profiles

	T (°C)	χ^2	Γ (mg m^{-2})	σ (nm)	δ_{rms} (nm)	δ_h (nm)	$\langle p \rangle$
$OE_{26}OB_{13}$	25	0.67	2.16	1.88	4.33	8.80	0.07
$OE_{29}OB_{11}$	25	0.44	1.87	1.89	3.66	8.40	0.15
	44	0.45	1.84	1.49	3.42	7.20	0.09
	62	0.53	1.69	1.71	3.42	7.60	0.15
$OE_{30}OB_{7}$	25	0.36	1.40	1.86	3.36	8.00	0.20
$OE_{27}OB_{6}$	25	0.49	2.23	1.34	2.46	6.00	0.28
	44	0.42	2.37	1.67	2.43	7.00	0.44
	62	0.27	2.32	1.07	1.74	5.00	0.48
$OE_{58}OB_{13}$	25	0.48	3.02	2.48	4.40	10.2	0.16
	44	0.57	3.02	2.23	3.54	9.20	0.28
	44	0.59	2.95	2.20	4.98	10.0	0.06
	62	0.42	2.98	2.12	4.02	9.20	0.15

Table 6. Parameters Derived from Model-Fitting Volume Fraction Profiles to the Scattering Data: Exponential-Type Profiles

	T (°C)	χ^2	Γ (mg m^{-2})	σ (nm)	δ_{rms} (nm)	δ_h (nm)	$\langle p \rangle$
$OE_{26}OB_{13}$	25	1.18	2.34	2.52	3.50	9.20	0.38
$OE_{29}OB_{11}$	25	0.48	1.98	2.36	3.27	8.80	0.40
	44	0.90	2.02	2.45	3.40	9.20	0.39
	62	0.53	1.79	1.76	2.42	7.20	0.50
$OE_{30}OB_{7}$	25	0.35	1.46	1.60	2.20	6.60	0.53
$OE_{27}OB_{6}$	25	1.07	2.40	2.16	2.98	8.20	0.43
	44	1.88	2.48	2.68	3.73	9.80	0.36
	62	1.69	2.69	3.49	4.87	11.8	0.29
$OE_{58}OB_{13}$	25	0.84	3.19	3.00	4.18	10.6	0.33
	44	1.98	3.27	3.17	4.42	11.0	0.32
	62	0.97	3.33	3.33	4.64	11.4	0.30

Table 7. Parameters Derived from Model-fitting Volume Fraction Profiles to the Scattering Data: Block + Exponential-Type Profiles (1 nm Wide Block at Surface)

	T (°C)	χ^2	Γ (mg m^{-2})	σ (nm)	δ_{rms} (nm)	δ_h (nm)	$\langle p \rangle$
$OE_{26}OB_{13}$	25	1.32	2.31	2.44	3.33	9.00	0.42
$OE_{29}OB_{11}$	25	0.47	1.93	1.67	2.27	6.80	0.55
	44	0.50	1.95	1.65	2.23	6.80	0.56
	62	0.54	1.76	1.39	1.89	6.00	0.62
$OE_{30}OB_7$	25	0.63	1.53	2.99	4.12	10.4	0.35
$OE_{27}OB_6$	25	1.37	2.36	2.16	2.95	8.20	0.46
	44	0.53	2.41	2.01	2.74	7.80	0.48
	62	0.62	2.46	2.25	3.08	8.60	0.44
$OE_{58}OB_{13}$	25	1.34	3.25	3.20	4.39	11.1	0.36
	44	0.73	3.13	2.58	3.52	9.46	0.40
	62	0.54	3.21	2.79	3.84	10.0	0.37

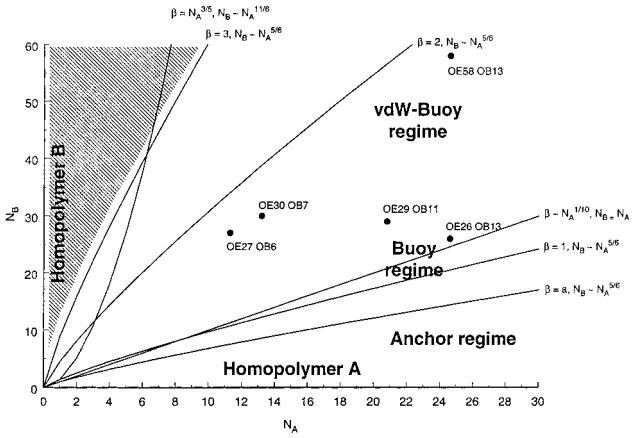

Figure 3. Diagrammatic representation of the adsorption phase space studied in this work. The positions of the different copolymers are also marked.

POE−POP−POE copolymers,[14,15] we noted that adsorbed amounts in perfluorocarbon emulsion systems were somewhat higher than those often recorded in particulate dispersions. The corresponding (effective hydrodynamic) layer thicknesses were 11, 16, and 29 nm for $OE_{41}OB_8$, $OE_{100}OB_{15}$, and $OE_{200}OB_{15}$ respectively. These values can be compared with the δ_h data from our profile fitting analysis in Tables 4−7. Again, there is a reasonable correspondence.

MJL envisage an adsorbed layer comprised of a thin but dense and poorly solvated layer of anchor blocks supporting a swollen layer of extended buoy blocks; a layer structure colloquially referred to as a *brush*. Different regimes are predicted depending on the magnitude of a block asymmetry parameter (for selective solvents) given by

$$\beta_{sel} = \frac{N_B^{3/5}}{N_A^{1/2}} a \qquad (4)$$

where N_A and N_B are the numbers of segments in the anchor (POB) and buoy (POE) blocks, respectively, and a is the ratio of the sizes of the repeat units (we have used the ratio of the cube roots of the molecular volumes giving $a = 0.81$). For more detail the reader is referred to the Appendix. Our assignment of the anchor and buoy blocks is based on our previous work with POE−POP−POE copolymers in this emulsion system. The corresponding phase space is shown in Figure 3 and the positions of the copolymers studied in this work have been marked. This figure was constructed in an analogous manner to that used by Hair et al. for the nonselective solvent case,[35] albeit for different copolymers.

In the *buoy regime* only the osmotic repulsion stretching the buoy blocks is important. In the *van der Waals−buoy (vdW−B) regime* the VdW energy of interaction between the surface and the anchor blocks competes with the stretching energy (defined in MJL's paper) of the buoy blocks. The transition between the two regimes is somewhat subjective but, according to MJL, occurs when β_{sel} is on the order of unity or, very roughly, when $N_A = N_B$. Different scaling behaviors are predicted in these two regimes, for example:

in the buoy regime

$$\theta \propto N_A^{12/25} N_B^{-30/25},$$
$$\delta_A \propto N_A^{37/25} N_B^{-30/25}, \delta_B \propto N_A^{4/25} N_B^{15/25}$$

in the VdW−buoy regime

$$\theta \propto N_A^{-12/23} N_B^{-6/23},$$
$$\delta_A \propto N_A^{11/23} N_B^{-6/23}, \delta_B \propto N_A^{-4/23} N_B^{21/23}$$

where δ_A and δ_B are the thicknesses of the anchor and buoy layers. Hence, $\delta_h \approx \delta_A + \delta_B$.

The calculated values of β_{sel} shown in Table 1 suggest that most of the copolymers should display behavior characteristic of the vdW−B regime. Copolymer $OE_{26}OB_{13}$, and possibly $OE_{29}OB_{11}$, could perhaps be in the bouy regime. To look for any correlations, the values of θ and σ derived from the surface-Guinier fits to the scattering data have been plotted as functions of the scaling relationships given above. The outcomes for the vdW−B regime are shown in parts a and b of Figure 4. Lines of regression, constrained to pass through the origin, have been added to guide the eye.

Concentrating first on the surface density data (Figure 4a), it is readily apparent that the MJL prediction for the vdW−B regime only partially explains these data. In particular, $OE_{30}OB_7$ appears to lie well outside any range of validity. However, this apparent anomaly can be readily understood once it is realized that $OE_{30}OB_7$ is the copolymer with the most isolated adsorbed chains (i.e., the largest value of D/R_g; see Table 3). It is then instructive to test the data against the scaling relationships for the buoy regime. These are shown in parts a and b of Figure 5. This time it is found that the outliers are $OE_{27}OB_6$ and $OE_{58}OB_{13}$; the copolymers exhibiting the greatest degree of steric interaction (smallest D/R_g values). Thus, we arrive at our first conclusions: (i) the data cannot be adequately explained by just one MJL regime, and (ii) the value of β_{sel} is not a reliable guide to the likely scaling behavior of the copolymers if there are significant variations in D/R_g. Significant in the present context means as little as 17% (the change from $OE_{26}OB_{13}$ to $OE_{27}OB_6$). Note that Figure 5a proves that it is not simply the case that neighboring chains must interact, that is $D/R_g \leq 1$, for the MJL description to be valid.

Turning to the second moment data in Figures 4b and 5b, one can see that there is very little to choose between the two scaling relationships. In addition, the effects of steric perturbation, discussed above, are not seen in these data. The likely explanation here is that because the MJL description was formulated for long copolymers, when N_B, and particularly N_A, are relatively small, the competing energetic contributions that are

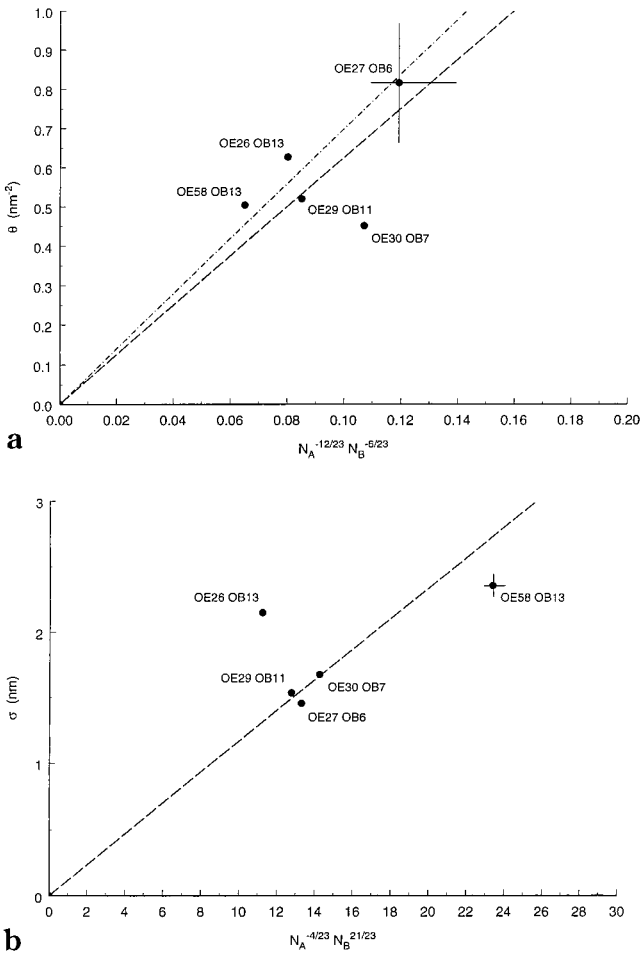

Figure 4. Comparison of the experimental data at 25 °C with the scaling predictions for the van de Waals−buoy regime: (a) surface density; (b) second moment of the layer thickness. Also shown are lines of regression: (− −) over all points and (− • −) excluding $OE_{30}OB_7$.

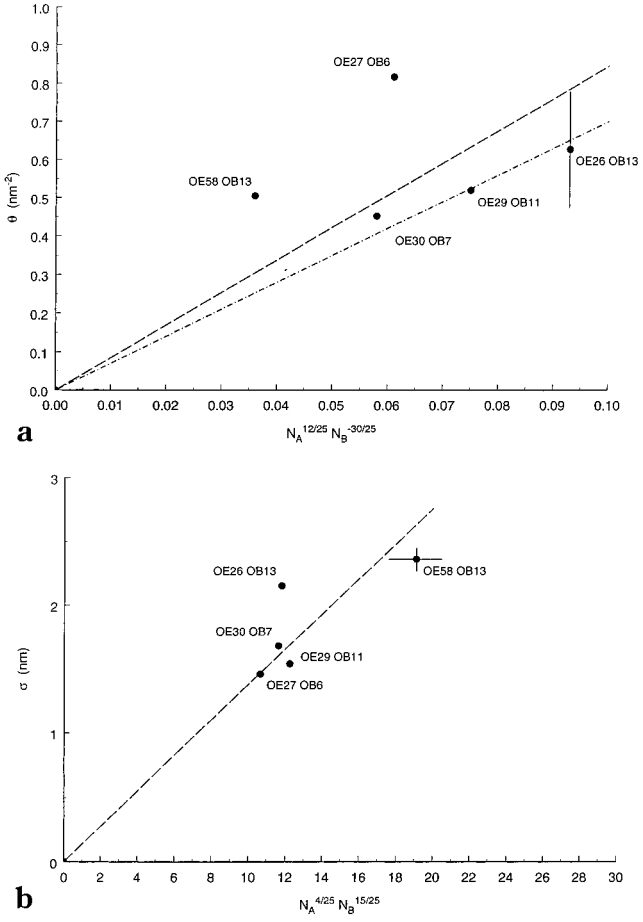

Figure 5. Comparison of the experimental data at 25 °C with the scaling predictions for the buoy-dominated regime: (a) surface density; (b) second moment of the layer thickness. Also shown are lines of regression: (− −) over all points and (− • −) excluding $OE_{58}OB_{13}$ and $OE_{27}OB_6$.

ultimately responsible for the adsorbed layer structure are more in balance, leading to rather ill-defined phase behavior.

A feature of our copolymers is that they have very short anchor blocks; in $OE_{27}OB_6$, the anchor is only six repeat units long. Previous experimental studies of brushlike adsorbed layers (with rather longer chains) have tended to avoid this situation because the copolymers would otherwise be highly asymmetric and thus outside the validity of the MJL description (such as the $OE_{200}OB_{15}$ copolymer studied by Griffiths et al.[34]). Consequently it is interesting to look at the effect of small anchors on the adsorbed layer structure. One obvious analogy that can be drawn is with terminally attached polymers (or adsorbed end-functionalized polymers). The scaling structure of adsorbed layers of terminally attached polymers has been described by Alexander−de Gennes.[36,37] Crucially the structure of these layers are also governed by the ratio D/R_g; when $D/R_g > 1$ polymer *mushrooms* are formed (so-called because the bulk of the polymer floats above a short tether) but these can be stretched into something reminiscent of a brush as D/R_g diminishes. Thus, the thickness of such an adsorbed layer depends on the surface density and the length of the solvated part of the chain. Theory predicts that, at fixed θ, σ should vary linearly with chain length or, at fixed chain length, as $\theta^{1/3}$. Hence, the product $\sigma\theta^{-1/3}$ should scale with the chain length. Such a plot is shown in Figure 6. Once again a line of regression constrained to pass through the origin has been added to guide the eye, but note that the data for $OE_{58}OB_{13}$ were deliberately omitted from the regression analysis since the experimental evidence indicates that this polymer forms a classic brushlike layer rather than a terminally attached layer. Within

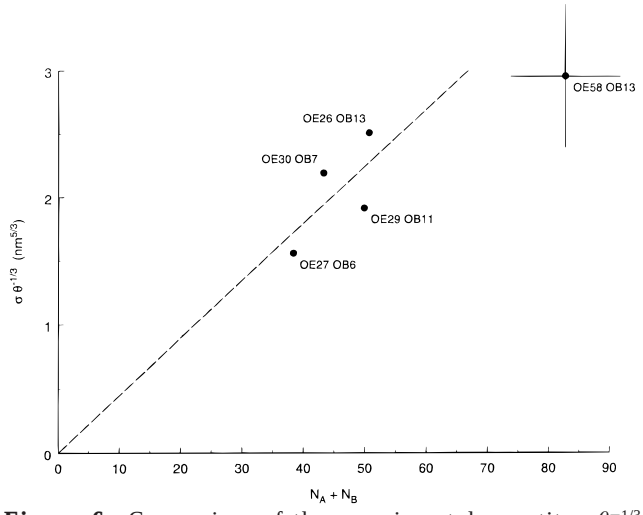

Figure 6. Comparison of the experimental quantity $\sigma\theta^{-1/3}$ derived from the 25 °C data with the overall chain length as suggested by the scaling prediction for the thickness of a grafted layer.

the error bounds of the data, there is a reasonable correlation. Displaying the data against just N_B (i.e., buoy block only), rather than $N_A + N_B$, shifts the graph to the left but otherwise does not significantly alter the finding. Our general conclusion is thus that $OE_{26}OB_{13}$, $OE_{29}OB_{11}$, $OE_{30}OB_7$, and $OE_{27}OB_6$ are forming rather weakly stretched brushlike layers which may emulate grafted chains but that $OE_{58}OB_{13}$ is more strongly stretched on account of its greater adsorption density and longer buoy blocks.

Volume Fraction Profiles. Several different possible architectures for the adsorbed layers have been discussed above, each of which can be characterized further through its corresponding volume fraction profile. Brushlike adsorbed layers give rise to profiles with a parabolic form when the buoy block is well-solvated and strongly stretched, but which become progressively block/steplike as solvency worsens. An exponential tail can be added to a block to allow for the small population of chains that remain more extended than the majority. On the other hand, terminally attached chains normally give rise to profiles with a maximum in polymer density just above the plane of the surface. These may be approximated by a Gaussian function. Highly collapsed layers, or layers in which the buoy blocks also adsorb, give rise to profiles that decay monotonically (approximately exponential-like). This latter type of profile is also encountered in the case of homopolymer adsorption, and even described the adsorbed layers formed by the POE−POP−POE triblock copolymers in our earlier work.[14,15]

To determine which profile types best fit the experimental data, it is necessary to compare the fitted values of Γ and σ in Tables 4−7 with the same values in Table 3. On the basis of our previous work, we expect the Γ data to be a far more sensitive test because they are related to the scattered intensity (which is measured on an absolute scale and can therefore be related to measurements by other techniques); the σ data simply describe how strongly the scattering decays with Q. We qualified our selections with the χ^2 parameter.

On this basis, we find that the best fit for $OE_{58}OB_{13}$ is obtained from the parabolic profile, confirming our preceding analysis of the surface-Guinier data. $OE_{26}OB_{13}$, $OE_{29}OB_{11}$, and $OE_{27}OB_6$ can be described almost equally as well by a parabolic profile as by a Gaussian profile, though on balance a parabolic profile is marginally better even if there are some inconsistencies in the extents of the layers. Perhaps not unsurprisingly, $OE_{30}OB_7$ is more problematic; it is difficult to choose between the parabolic, Gaussian, and exponential profiles in this instance. One thing that is quite clear, however, is that with the possible exception of $OE_{30}OB_7$, profiles with a concave curvature are rather poor at representing the data (observe also that the profile shown in the inset in Figure 2 has a roughly convex form). This fact alone supports our hypothesis that the copolymers form thin brushlike adsorbed layers but with a considerable variation in the degree of stretching. Like Schillen et al.,[33] we also note that the overall extents of the profiles (δ_h) are comparable to the lengths of helical POE conformers of the same number of POE units; approximately given by $l_{helix} = 0.095 \times 3N_{OE}$ nm.[38] In fact, the ratio R_g/l_{helix} actually diminishes as the asymmetry of the copolymer (i.e., β_{sel}) increases. In other words, when EO buoy blocks are purely osmotically stretched (buoy regime) their extent can be well approximated by l_{helix}; however, this correlation becomes less sound as the asymmetry of the copolymer forces it into the vdW−buoy regime.

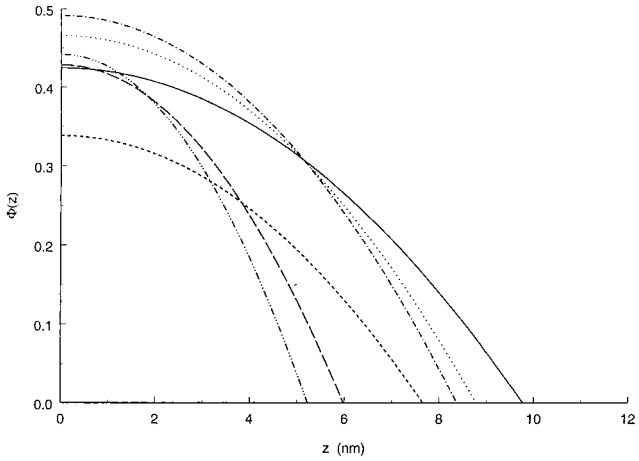

Figure 7. Best-fit parabolic volume fraction profiles for $OE_{29}OB_{11}$ and $OE_{58}OB_{13}$ obtained at three different temperatures. $OE_{58}OB_{13}$: (—) 25 °C; (· · ·) 44 °C; (— · —) 62 °C. $OE_{29}OB_{11}$: (— —) 25 °C; (— —) 44 °C; (· · · — · · ·) 62 °C.

Griffiths et al.[34] found that exponential profiles best described the adsorbed layers formed by $OE_{100}OB_{15}$ and $OE_{200}OB_{15}$ on polystyrene latex, but in their experiments *both* blocks were free to adsorb even though only the POE block was solvated. This difference in volume fraction profile types actually supports our assertion that in our systems only the POB segments adsorb.

Bound Fractions. In an *ideal* brush the bound fraction should equate with the anchor block content of the copolymers, $\nu_A = (1 - \nu_B)$. For the copolymers studied here, $0.29 \leq \nu_A \leq 0.49$; see Table 1. If we compare these values with the bound fractions derived from the fitted parabolic profiles (Table 4), we find that, with the exception of $OE_{27}OB_6$, the experimental bound fractions are only 40−70% of ν_A. Further inspection shows that it is the copolymers with the most anchor blocks that exhibit the greatest discrepancy. This may be an indication that only relatively few OB repeat units are necessary to anchor each copolymer molecule and that above this number ($N_{OB} \approx 6$) the anchor blocks are more looped. Gaussian profiles give bound fractions that are rather smaller than ν_A, while exponential-based profiles give bound fractions that are somewhat larger.

Effect of Temperature. Considering the surface-Guinier data in Table 3, it would appear that for a given copolymer θ (or Γ) is independent of temperature. However, in the case of $OE_{27}OB_6$ and $OE_{58}OB_{13}$, there is clear evidence that σ shrinks as the temperature is raised. This trend is echoed in the data from the model fits to the parabolic profiles (Table 4). Figure 7 shows how the form of the profiles for $OE_{29}OB_{11}$ and $OE_{58}OB_{13}$ changes with temperature. As the temperature is raised, the buoy layer contracts, but at the same time, there is an increase in the number density of copolymer segments in the vicinity of the surface and consequently in the bound fraction. For $OE_{29}OB_{11}$ and $OE_{27}OB_6$ $\langle p \rangle$ increases between 25 and 62 °C by 43% and 25% respectively, but in the case of $OE_{58}OB_{13}$, the change is much smaller, about 6%. Given that these changes are not accompanied by any comparable change in the adsorbed amounts, the reduction in the layer thicknesses must come about as the result of steric rearrangements deep inside the layer rather than at the

interface with the dispersion medium. The smaller change in the case of $OE_{58}OB_{13}$ is probably related to the stronger stretching of its buoy block.

The profiles themselves decay more sharply at the higher temperatures (i.e., becoming more blocklike). This behavior is qualitatively similar to that predicted by the SCF calculations of Wijmans and Zhulina, which consider the effect of decreasing solvent quality on a brush.[39] Their predictions would be consistent with a progressive temperature-induced dehydration of the OE segments in our system, for which there is considerable experimental evidence in the literature.[40,41] Interestingly we did not see similar behavior in our earlier work with POE−POP−POE copolymers, although as already mentioned these did not form brushlike layers.

Raising the temperature from 25 to 44 °C appears to have a much bigger effect on the layer structure than an increase from 44 to 62 °C. Since the cloud points of our copolymers in water are well in excess of 62 °C, this effect may actually owe more to changes in the adsorption of the OB blocks than it does to dehydration of the OE blocks. An analogy can be drawn with the micellization of POE−POP−POE copolymers where in some instances the hydrophobic effect—the hydrogen bonding of water to itself—is much more important than the hydrogen bonding of water to the ether oxygens in the OE blocks.[10,18]

Summary

In this paper we have used small-angle neutron scattering data to provide detailed information about the structure of the adsorbed layers formed by five short-chain diblock copolymers of poly(oxyethylene) and poly(oxybutylene) for which $N_{OE} \gg N_{OB}$ (i.e., $N_B > N_A$). It is the poly(oxybutylene) blocks which anchor the adsorbed chains at the interface, in this case between a perfluorocarbon oil dispersed phase and water.

Provided that the effective distance between adsorbed chains at the interface is less than the corresponding radius of gyration, the adsorbed layer structure can be reasonably well described as a brush, though we conclude that there are significant variations in the degree of stretching of the poly(oxyethylene) buoy blocks. When the adsorbed chains are more isolated, the brushlike structure is less apparent and even, due to the rather asymmetric nature of our copolymers, reflects signs of the mushroomlike behavior normally associated with terminally attached chains.

We have also found that theoretical descriptions of the adsorption behavior, such as the scaling theory of Marques, Joanny, and Leibler, are unable to unambiguously predict the adsorption behavior of our copolymers, even when $\beta_{sel} > 1$. We attribute this to their short chain length (and thus more balanced energetic contributions between adsorption and stretching).

Increasing the temperature has the effect of reducing solvent quality for the buoy blocks, and results in a shift of segment density toward the surface. However, as the adsorbed layers contract, there is a negligible change in the amount of copolymer actually adsorbed. Together, these factors imply a temperature-induced structural rearrangement near the copolymer junction and not simply a dehydration of the periphery of the brush.

Acknowledgment. The authors would like to thank the Engineering and Physical Sciences Research Council for support and the Central Laboratory of the Research Councils ISIS Facility for the provision of neutron scattering facilities. S.M.K. would also like to thank Dr. John Hone of the University of Bristol for teaching him how to use the profile fitting program. Y.-W.Y. thanks the Government of the People's Republic of China for the provision of a research studentship.

Appendix

Here we wish to emphasize the distinction between certain theoretical parameters and their physical analogues.

Implicit in the MJL description is the (Flory) assumption that each anchor or buoy *segment* occupies the same volume; i.e., $a = 1$. Of course, this may not be reflected experimentally and chemically distinct *repeat units* may have different volumes, as is the case with OE and OB.

Mai et al.[42] have shown that if one takes the volume occupied by an OE unit as a reference, then the volume occupied by an OB unit is 1.89 times larger. This difference is *independent* of temperature.

Hence we may deduce that (i) $a = 3\sqrt{(1/1.89)} \approx 3\sqrt{(44.05/1.127)/(72.10/0.975)}$, (ii) $N_A = 1.89N_{OB}$, and (iii) $N_B = N_{OE}$.

Note also that in some of the other literature involving POE/POB copolymers, N_{OE} is denoted as m and N_{OB} is denoted as n.

References and Notes

(1) Fleer, G. J.; Cohen-Stuart, M. A.; Scheutjens, J. M. H. M.; Cosgrove, T.; Vincent, B. *Polymers at Interfaces*; Chapman & Hall: London, 1993.
(2) Everett, D. H. *Basic Principles of Colloid Science*; Royal Society of Chemistry: London, 1988.
(3) Tomlinson, E., Davis, S. S. Eds. *Site-Specific Drug Delivery*; John Wiley: Chichester, England, 1986.
(4) Chu, B. *Langmuir* **1995**, *11*, 414.
(5) Almgren, M.; Brown, W.; Hvidt, S. *Colloid Polym Sci.* **1995**, *273*, 2.
(6) Malmsten, M.; Linse, P.; Cosgrove, T. *Macromol.* **1992**, *25*, 2474.
(7) Shar, J. A.; Obey, T. M.; Cosgrove, T. *Colloid Surf.* **1998**, *136*, 21.
(8) Yu, G.-E.; Masters, A. J.; Heatley, F.; Booth, C.; Blease, T. G. *Macromol. Chem. Phys.* **1994**, *195*, 1517.
(9) Yu, G.-E.; Altinok, H.; Nixon, S. K.; Booth, C.; Alexandridis, P.; Hatton, T. A. *Eur. Polym. J.* **1997**, *33*, 673.
(10) Yu, G.-E.; Deng, Y.-L.; Dalton, S.; Wang, Q.-G.; Attwood, D.; Price, C.; Booth, C. *J. Chem. Soc., Faraday Trans.* **1992**, *88*, 2537.
(11) Bedells, A. D.; Arafeh, R. M.; Yang, Z.; Attwood, D.; Padget, J. C.; Price, C.; Booth, C. *J. Chem. Soc., Faraday Trans.* **1993**, *89*, 1235.
(12) Yang, Y.-W.; Yang, Z.; Zhou, Z.-K.; Attwood, D.; Booth, C. *Macromolecules* **1996**, *29*, 670.
(13) Kelarakis, A.; Havredaki, V.; Derici, L.; Yu, G.-E.; Booth, C.; Hamley, I. W. *J. Chem. Soc., Faraday Trans.* **1998**, *94*, 3639.
(14) Washington, C.; King, S. M.; Heenan, R. K. *J. Phys. Chem.* **1996**, *100*, 7603.
(15) Washington, C.; King, S. M. *Langmuir* **1997**, *13*, 4545.
(16) Yu, G.-E.; Yang, Z.; Ameri, M.; Attwood, D.; Collett, J. H.; Price, C.; Booth, C. *J. Phys. Chem. B* **1997**, *101*, 4394.
(17) Cohen-Stuart, M. A.; Waajen, F. H. W. H.; Cosgrove, T.; Vincent, B.; Crowley, T. L. *Macromolecules* **1984**, *17*, 1825.
(18) Kelarakis, A.; Havredaki, V.; Yu, G.-E.; Derici, L.; Booth, C. *Macromolecules* **1998**, *31*, 944.
(19) Davis, S. S.; Round, H. P.; Purewal, T. S. *J. Colloid Interface Sci.* **1981**, *80*, 508.
(20) http://www.isis.rl.ac.uk.
(21) Heenan, R. K.; Penfold, J.; King, S. M. *J. Appl. Crystallogr.* **1997**, *30*, 1140.
(22) Heenan, R. K.; King, S. M.; Osborn, R.; Stanley, H B, *COLETTE Users Guide*; Rutherford Appleton Laboratory Report RAL-89-128; 1989. King, S. M.; Heenan, R. K. *Using COLETTE*; Rutherford Appleton Laboratory Report RAL-95-005, 1995.

(23) Wignall, G. D.; Bates, F. S. *J. Appl. Crystallogr* **1987**, *20*, 28.
(24) Cosgrove, T.; Crowley, T. L.; Vincent, B.; Barnett, K. G.; Tadros, Th. F. *Structure of the Interfacial Region*; Faraday Symposia of the Chemical Society, No 16; Chemical Society: London, 1981.
(25) King, S. M.; Griffiths, P. C.; Cosgrove, T. In *Applications of Neutrons in Soft Condensed Matter*; Gabrys, B. J., Ed.; Gordon & Breach: London, in press.
(26) Cosgrove, T. *J. Chem. Soc., Faraday Trans.* **1990**, *86*, 1332.
(27) Crowley, T. L. D.Phil. Thesis, University of Oxford, England, 1984.
(28) Cosgrove, T. Unpublished work.
(29) Cosgrove, T.; Ryan, K. *Langmuir* **1990**, *6*, 136.
(30) Scheutjens, J. M. H. M.; Fleer, G. J. *J. Phys. Chem*. **1979**, *83*, 1619.
(31) Scheutjens, J. M. H. M..; Fleer, G. J. *J. Phys. Chem*. **1980**, *84*, 178.
(32) Marques, C.; Joanny, J. F.; Leibler, L. *Macromolecules* **1988**, *21*, 1051.
(33) Schillen, K.; Claesson, P. M.; Malmsten, M.; Linse, P.; Booth, C. *J. Phys. Chem. B* **1997**, *101*, 4238.
(34) Griffiths, P. C.; Cosgrove, T.; Shar, J.; King, S. M.; Yu, G.-E.; Booth, C.; Malmsten, M. *Langmuir* **1998**, *14*, 1779.
(35) Guzonas, D. A.; Boils, D.; Tripp, C. P.; Hair, M. L. *Macromolecules* **1992**, *25*, 2434.
(36) de Gennes, P. G. *J. Phys.* **1976**, *37*, 1443.
(37) Alexander, S. *J. Phys.* **1977**, *38*, 983.
(38) Craven, J. R.; Zhang, H.; Booth, C. *J. Chem. Soc., Faraday Trans.* **1991**, *87*, 1183.
(39) Wijmans, C. M.; Zhulina, E. B. *Macromolecules* **1993**, *26*, 7214.
(40) Saeki, S.; Kuwahara, N.; Nakata, M.; Kaneko, M. *Polymer* **1976**, *17*, 685.
(41) King, S. M.; Heenan, R. K.; Cloke, V. A.; Washington, C. *Macromolecules* **1997**, *30*, 6215 and the references therein.
(42) Mai, S.-M.; Booth, C.; Nace, V. M. *Eur. Polym. J*. **1997**, *33*, 991.

MA990730V